

# Improving the effective temperature estimation over sea ice using low frequency microwave radiometer data and Arctic buoys

Lise Kilic

June 29, 2017

## 1 Introduction

The objective is to improve the estimation of the sea ice effective temperature which is part of the sea ice emissivity (OSI-404) product and which could potentially be used for improving the physical correction of sea ice concentration (OSI-401-b). This will be achieved by deriving empirical relationships (regression models) for the snow-ice interface temperature and the effective temperature as a function of the AMSR brightness temperatures. The snow ice interface temperature is strongly correlated with the Teff.

The Teff is the integrated emitting layer temperature of the snow and ice. Teff is related to the upper profile physical snow and ice temperature by the snow and ice microwave emission and scattering processes [Tonboe et al., 2011]. These relationships between Teff and the physical temperature profile are complicated especially at higher microwave frequencies ( $> 10GHz$ ) where scattering from snow grains and voids in the sea ice plays an important role. Also layering and vertical structure in the snowpack is affecting the microwave emission processes and especially the polarisation difference of the brightness temperature (Tb) at horizontal polarisation [Tonboe, 2010]. Because of these complicated relationships between the physical temperature, Teff and the brightness temperature an empirical algorithm based on regression analysis will be pursued using the extensive sea ice buoy and in situ database developed in the ESA sea ice CCI project (<http://www.seaice.dk/ecv2/rrdb-v1.1/>).

At 6 GHz there is a very high linear correlation between the snow-ice interface temperature and the Tb and Teff [Tonboe et al., 2011]. This is because the microwave penetration through the snow layer and because the emission is relatively unaffected by scattering from snow grains. Higher frequencies have more shallow penetration than at 6 GHz due to increasing scattering and absorption as a function of frequency and preliminary results show that it is possible to derive the vertical temperature profile using a suite of frequencies and simple regression models [Grönfeldt, 2015]. Even though these relationships get more noisy at higher microwave frequencies ( $> 10GHz$ ) there is still a very high correlation between Teff at microwave channels between 6 and 50 GHz [Tonboe et al., 2011]. This is exploited in the current operational set-up for deriving Teff in OSI-404-a (yet unpublished but updated ATBD).

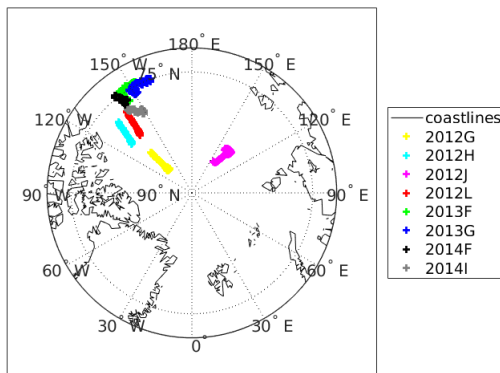
In section 2 a description of the dataset used will be given, then in section 3, the method used to estimate the snow-ice interface temperature, the snow depth and Teff is presented, and in section 4 the results will be shown and discussed.

## 2 Dataset

### 2.1 The Round Robin Database

The European Space Agency's (ESA) climate change initiative (CCI) sea ice project has established a round robin data package (RRDP) for sea ice concentration (SIC) algorithm inter-comparison and evaluation. The dataset is openly available. It contains an extensive collection of collocated microwave radiometer data and other geophysical parameters with relevance for computing and understanding variability of the

Figure 1: Position of IMB buoys over Arctic



microwave radiometer SIC over open water and 100% sea ice. The RRDP contains data which can be used for analysing SIC variability and the microwave emission processes and their relationship with the snow and ice temperature, snow cover and ice. It can therefore also be used for analysing other sea ice parameters than SIC, here, the temperature.

In the RRDP we will look at the Ice Mass Balance (IMB) Buoys data and at the Operation Ice Bridge (OIB) data collocated with the observations of the radiometer Advance Microwave Scanning Radiometer -2 (AMSR-2).

## 2.2 AMSR data

In the RRDP, in-situ data are collocated with the observations from AMSR-E (May 2002 - October 2011) or AMSR-2 ( May 2012 - now ) depending on the year. AMSR-2 is a passive microwave radiometer sensor. The instrument is on board JAXA's GCOM-W1 satellite, launched on May 18, 2012. AMSR-2 has 14 channels : 6.9, 7.3, 10.65, 18.7, 23.8, 36.5 and 89 GHz for both vertical and horizontal polarization. The products of this sensor are brightness temperatures for each channel. The spatial resolution of each of the channels has been resampled to the 6 GHz resolution before co-location (RRDP report Pedersen and Saldo [2016]).

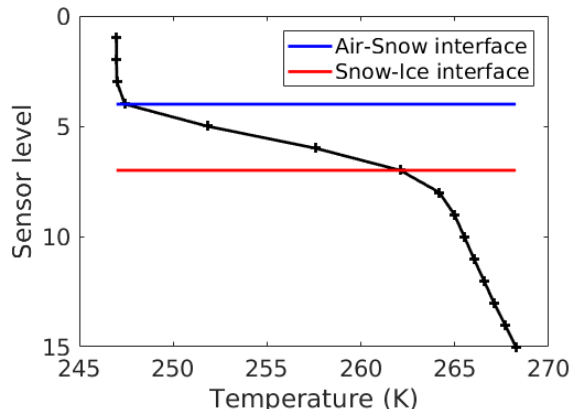
## 2.3 CRREL Ice Mass Balance Buoy Data

Ice mass balance (IMB) buoys are installed to measure the ice mass balance of the Arctic sea ice cover. Buoy Components include an above ice acoustic sounder, under ice acoustic sounder, and a temperature string extending from the air, through the snow cover and sea ice, into the water with the temperature sensors located every 10 cm along the string. The buoys also include instruments to measure air temperature, barometric air pressure and GPS position. A data acquisition system collects and transmits the data back to CRREL (Cold Regions Research and Engineering Laboratory) [Perovich et al., 2017].

In the RRDP the IMB buoys data were collocated with : ERA-interim which is reanalysis data using Numerical Weather Prediction (NWP) and delivered by ECMWF (European Centre for Medium-Range Weather Forecasts) [Berrisford et al., 2011], the brightness temperatures from the microwave radiometer AMSR-2 or AMSR-E, and ASCAT observations. The scatterometer data are from IFREMER CERSAT. In the new version (v1.91) of the RRDP, there is also SMOS, SMAP and QSCAT observations collocated with the IMB buoys.

For this study, I use buoy data recorded during the cold period during winter (1st December to 1st April). During the first part of the study I used the buoys : 2012 G, 2012 H, 2012 J and 2012 L. Later during the study the RRDP was updated and four new buoys were included: 2013 F, 2013 G, 2014 F and 2014 I.

Figure 2: Temperature profile from IMB buoy 2012 G with air-snow interface level and snow-ice interface level computed with automated method



## 2.4 Operation Ice Bridge data

Since 2009 NASA’s Operation Ice Bridge has collected ice and snow thickness data in the Arctic during annual flight campaigns (March- May) to bridge the gap between ICESAT1 (2003-2010) and ICESAT2 (planned launch in 2018) satellite missions. The data are especially valuable in this context since they contain snow thickness information from the snow radar. In RRDP, original OIB data are averaged into 50 km sections for better overlap/co-location with AMSR TB data. OIB data are also collocated with AMSR-2/AMSR-E observations, ASCAT observations and ERA-interim reanalysis data.

## 2.5 Simulated data from MEMLS model

Simulations were performed using the MEMLS model [Mätzler and Wiesmann, 2012]. Effective temperature and emissivity of sea ice at different frequencies were computed from different snow and ice parameters.

# 3 Methods

Here I describe step by step, the method used in order to improve the sea ice effective temperature estimate. We will look at a snow-ice interface temperature level detection method. Then we will describe our method to retrieve the snow-ice interface temperature, the snow depth and finally the effective temperature.

## 3.1 Temperature profile through snow and ice

Sea ice temperature profile have particular behavior. The temperature starts very cold in the air during winter. In the snow, temperature gets warmer as a function of the depth. The temperature gradient in the snow is very large. In ice, the temperature gradient becomes smaller than in the snow because of differences in the snow and ice thermal conductivity, but the temperature still to get warmer as a function of the depth. Then in water, where the temperature is just the freezing point, the temperature gradient is very small in the upper meter because of turbulent mixing.

Air-snow interface and snow-ice interface position can be detected by a change in the temperature gradient. An automated method was implemented (Matlab code is given in Appendix A.1). It detects the slope changes in the temperature profile. Figure 2 shows a typical temperature profile through sea ice from IMB buoy 2012 G and the air-snow interface and snow-ice interface positions deduced with the automated method.

Figure 3: Correlation coefficient  $R$  between AMSR-2 channels and the physical temperature at different depth levels. IMB buoy 2012 J.

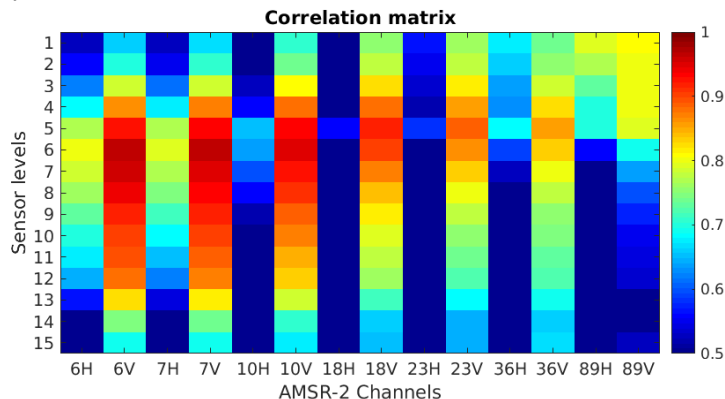
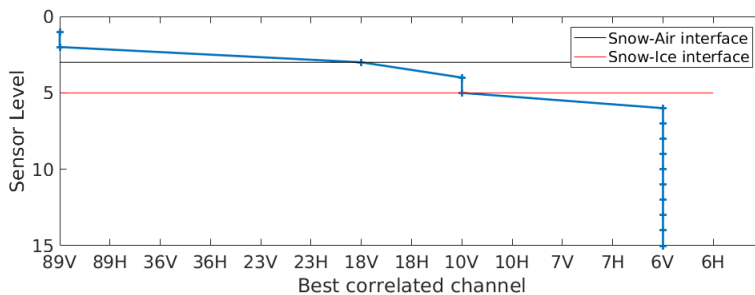


Figure 4: The most correlated channel to the physical temperature at each depth level through air, snow and ice. At each depth level the channel giving the highest correlation coefficient is indicated. IMB buoy 2012 J.



For each buoy, the snow-ice interface level is the mean on the entire winter period, of the snow-ice interface levels detected for each profile recorded by the buoy. The same is done for the air-snow interface level. This makes it possible not to take into account some particular profiles but the variability of the snow-ice interface position and snow-air interface position during winter is not taken into account.

### 3.2 Forward selection method

To retrieve the snow-ice interface temperature from brightness temperature at low microwave frequency, statistical analysis have been made to select the channels which are best describing the variability of the snow-ice interface temperature. Correlation coefficient between the temperature at each level of depth and the brightness temperature at each frequency is computed (see Figure 3). Note that the brightness temperature of horizontal polarization are less correlated with the physical temperature than the brightness temperature at vertical polarization.

Figure 4 shows the best correlated channel for each depth level. The 89 GHz V-pol channel brightness temperature is well correlated with the air temperature. The 6 GHz V-pol channel brightness temperature is well correlated with the ice temperature as expected. Note that at snow-ice interface it is the 10 GHz V-pol channel which is the best correlated channel.

The *stepwisefit* function from MATLAB was used to select the most relevant channels when using more than one channel for the regression.

### 3.3 Multi-linear regressions

#### 3.3.1 Snow-ice interface temperature from brightness temperature

According to the results found in the section 3.2, the 10.65 GHz V-pol channel is the most correlated channel to the temperature at the snow-ice interface and it will be used to retrieve the TSI. The 6.9 GHz channel will also be used to retrieve TSI because it is high correlated to temperature at the snow-ice interface. A comparison will be done between the regression using 10.65 GHz channel and the regression using 6.9 GHz channel.

The buoys 2012G, 2012H, 2012L are used to do the linear regression. The buoy 2012 J has a large dispersion of its TSI observations in a small brightness temperature range, therefore this buoy is not used to do the regression.

In a first method, the data are centered, and a linear equation is computed for each buoy between the snow-ice interface temperature and the brightness temperature at 10.65 GHz in V-pol. A mean is done with the coefficients from the different buoys and a coefficient of the slope of  $1.667 \pm 0.3844$  was found. Another method can be applied it consists of doing the linear regression on the centered data of all buoys, thus the coefficient of the slope found is  $1.101 \pm 0.028$ . With 6.9 GHz V-pol channel, the coefficient for the first method is  $1.209 \pm 0.39$  and for the second is  $1.144 \pm 0.032$ . The second method is more robust than the first one considering the estimation errors. In the following, the coefficients from the second method are used.

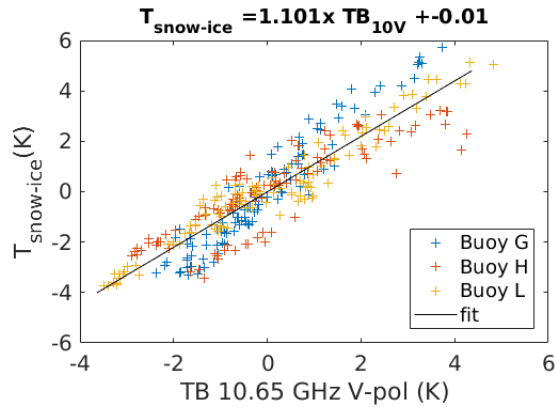


Figure 5: Centered TSI expressed as a function of the centered TB at 10.65 GHz. Data from the buoys are in colored points and the linear regression is the black line.

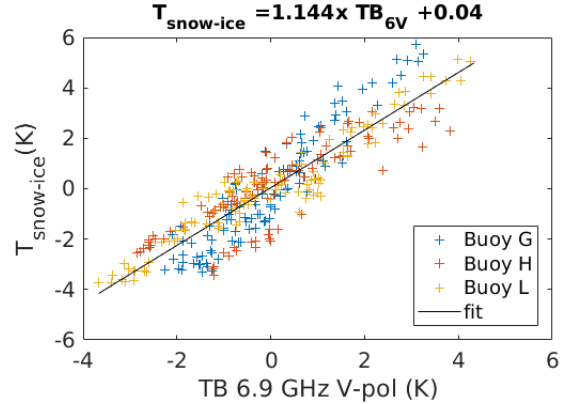


Figure 6: Centered TSI expressed as a function of the centered TB at 6.9 GHz. Data from the IMB buoys are in colored points and the linear regression is the black line.

#### 3.3.2 Snow-ice interface temperature from snow depth

Without center the data, the offset of linear regression is not the same for each buoy. A linear relation between the inverse of snow depth and the snow ice interface temperature is found to explain the changing offset.

This dependence of the TSI as a function of the inverse of the SD is explained physically. The temperature gradient in the snow can be expressed as follows [Sturm et al., 2002] :

$$\frac{dT_s}{dz} = \frac{T_{air} - TSI}{SD} \quad (1)$$

where  $T_s$  is the temperature in the snow,  $z$  the depth and  $T_{air}$  the air temperature. Integrating the equation

1, we obtain :

$$\int SDdT_s = \int (T_{air} - T_{SI})dz \quad (2)$$

$$T_s = \frac{(T_{air} - T_{SI})}{SD}z + \frac{C}{SD} \quad (3)$$

Where C is a constant. If  $T_s = T_{SI}$  then  $z = SD$ , the TSI is finally expressed as a function of the inverse of snow depth :

$$T_{SI} = \frac{T_{air}}{2} + \frac{C}{SD} \quad (4)$$

In order to compute the coefficient of our linear regression between snow depth ( $SD$ ) and snow-ice interface temperature, the snow-ice interface temperature ( $T_{SI}$ ) is corrected of its brightness temperature ( $TB$ ) dependence as follows :

$$T_{SI} - a \times TB = b \times \frac{1}{SD} + c \quad (5)$$

Then linear regression is done between snow-ice interface temperature and the inverse of snow depth with the data from all IMB buoys (2012 G, H, J, L, 2013 F, G and 2014 F, I). Results at 6.9 GHz and 10.65 GHz will be shown in section 4.1.

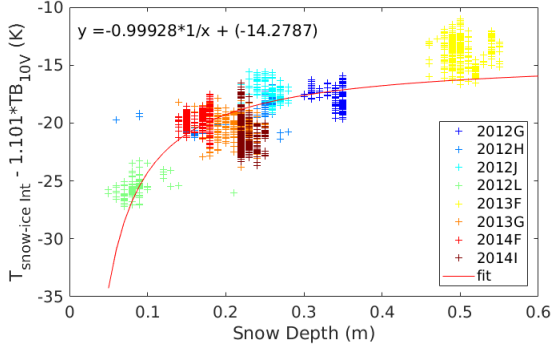


Figure 7: TSI corrected of the TB at 10.65 GHz dependence as function of the snow depth. Datas from the different IMB buoys are in colored points and the regression is the red line.

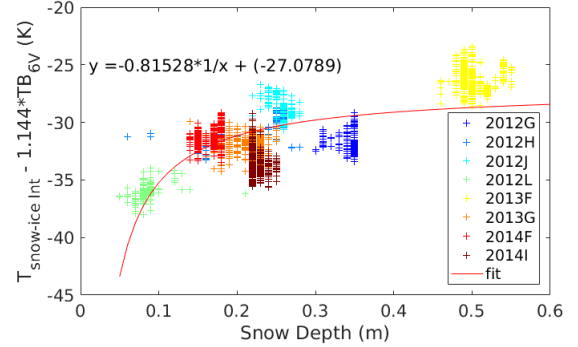


Figure 8: TSI corrected of the TB at 6.9 GHz dependence as function of the snow depth. Datas from the different IMB buoys are in colored points and the regression is the red line.

### 3.3.3 Snow depth from brightness temperature

We would like to estimate the snow-ice interface temperature from satellite brightness temperature. The snow-ice temperature is depending on snow depth, an analysis is done to estimate the snow depth from brightness temperatures. First the OIB data from the campaign of 2013 are used to do the forward selection of channels. OIB data permit to have enough observations to do our analysis. The gradient ratio between the channels 19 GHz and 37 GHz V-pol is known to retrieve the snow depth [Markus and Cavalieri, 1998, Comiso et al., 2003], but it doesn't show good results for our case. It has been developed for snow on Antarctic first-year ice and it overestimates snow depth over Arctic multiyear ice. Using the function stepwisefit from MATLAB, the best channels found to retrieve the snow depth variability are the 6.9 GHz V-pol, 18 GHz V-pol and 36.5 GHz V-pol.

Then the multilinear regression is done using the IMB data from the winter 2012-2013 (Buoys 2012 G,H,J,L).

$$SD = d \times TB_{6V} + e \times TB_{18V} + f \times TB_{36V} + g \quad (6)$$

Results will be shown in section 4.2.

The multi-linear regressions using 2 predictors (18.7 and 36.5 GHz channels) and using 4 predictors (6.9, 18.7, 36.5 and 89 GHz channels) have been also tested. But the results obtained with these combinations increase the RMSE when comparing with IMB buoys data and the independent OIB data.

### 3.3.4 Effective temperature from Snow-Ice interface temperature

The effective temperature is only available on data simulated with the MEMLS model. The simulations were part of an earlier version of the RRDP and the simulation methodology is described in Tonboe [2010]. The empirical linear equations 8 and 9 found with observation data are compared with simulated data. A bias is expected between the model and the observations. Snow-ice interface temperature from simulated data and snow-ice interface temperature from observations are therefore related as follows if slopes are similar:

$$TSI_{sim} = TSI_{obs} + offset \quad (7)$$

Then a linear relation between the effective temperature at different channels and the snow-ice interface temperature is computed using only simulated data. For each channel linear regression is done between the effective temperature in vertical polarization and the snow-ice interface temperature. Results will be described in section 4.3.

## 4 Results and Discussion

### 4.1 Snow-Ice interface Temperature

The final equations to relate snow-ice interface temperature to the snow depth and the brightness at 10.65 GHz on the one hand and at 6.9GHz on the other hand are presented here :

$$T_{SI} = 1.101 \times TB_{10V} - 0.999 \times \frac{1}{SD} - 14.28 \quad (8)$$

$$T_{SI} = 1.144 \times TB_{6V} - 0.815 \times \frac{1}{SD} - 27.08 \quad (9)$$

Where TSI and TB are expressed in K, and SD in m.

The Root Mean Squared Error is calculated for the two linear regressions using the observations of the 8 IMB buoys available. The RMSE for the linear regression using the 10 GHz channel is 2.11 K and for the linear regression using the 6.9 GHz channel is 2.22 K. The 10 GHz channel better describe the variability due to the snow depth (see Figures 9 and 10). In Figure 9 and 10, the straight line is representing TSI calculated from the equations 8 and 9 respectively, where SD is taken as the mean of the SD measuring by the buoy during the entire winter. The channel giving the closest results to the observations is not always the same, depending on the buoy and other parameters (see Figure 11). Some errors can be introduced when choosing the level of the snow-ice interface. In the methodology the level of the snow-ice interface is chosen constant during the time within the same buoy. So, possible changes of the position of the snow ice interface are not taken into account. Moreover, vertical resolution of the IMB buoys is 10 cm, which can introduce some errors too. Correcting for these effects will improve the accuracy of the model.

### 4.2 Snow Depth

The multiple linear regression to retrieve the snow depth from brightness temperature is expressed as follows:

$$SD = 1.7701 + 0.017462 \times TB_{6V} - 0.02801 \times TB_{18V} + 0.0040926 \times TB_{37V} \quad (10)$$

Where SD is expressed in m and TB in K.

To calculate the RMSE all IMB buoys have been used except the 2013 F buoy which have a very deep snow ( $> 0.5m$ ). The RMSE is 0.0512 m.

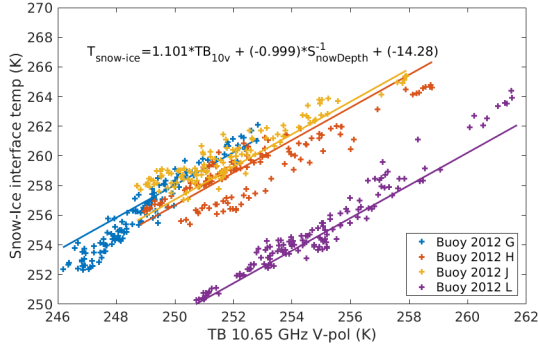


Figure 9: Snow-Ice interface temperature expressed as function of brightness temperature at 10.65 GHz, for the different IMB buoys. Observations are in colored points and the linear regression in colored straight line. The mean snow depth of the buoy is used to compute  $T_{snow-ice}$  with the linear model.

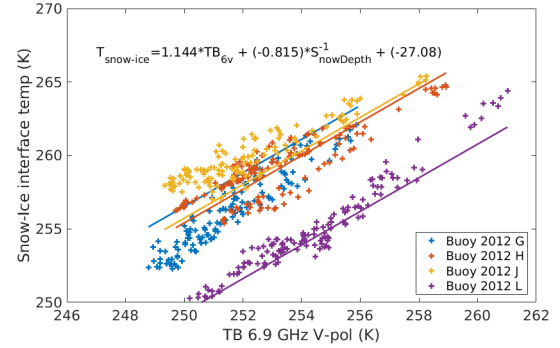
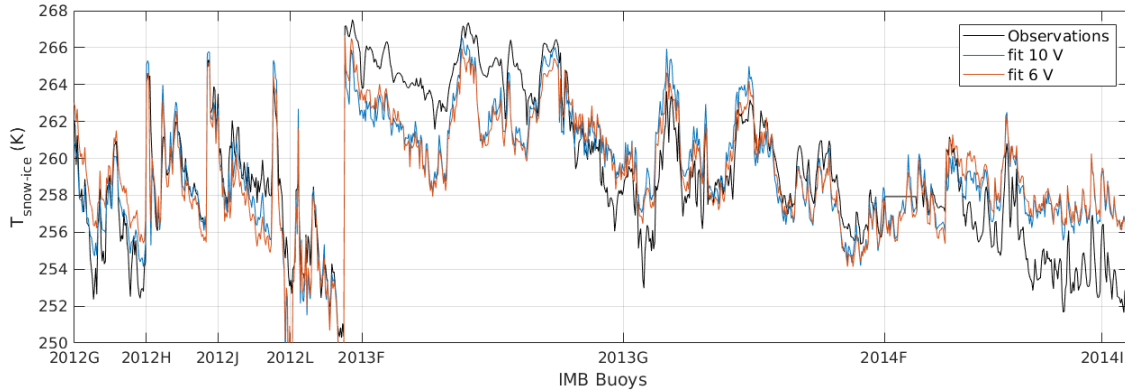


Figure 10: Same than Figure 9 but using 6.9 GHz brightness temperature

Figure 11: Comparisons between the observations from the different IMB buoys and the linear regressions with the 10 GHz channel and 6 GHz channel.



We also compare the results of the multiple linear model with the measurements from the OIB campaign during the year 2013. The RMSE between OIB data and the multiple linear model is 0.0626 m. Figure 13 shows a very good consistency between the observations and the simulations. The correlation coefficient calculated worth  $r = 0.86$ .

This model shows encouraging results but it doesn't work for too thin snow ( $< 0.05m$ ) nor for too deep snow ( $> 0.5m$ ).

### 4.3 Sea Ice Effective Temperature

Finally, we use a dataset of simulated effective temperature using the MEMLS model in order to find the relation between the snow-ice interface temperature and the effective temperature at different channels.

The equations 8 and 9 are tested on the simulated data from MEMLS. Figures 14 and 15 show the results of this comparison. The offset of our multi-linear regression was read from the figure manually on the MEMLS simulated data. A bias of 5 K is found between the snow-ice interface temperature estimated

Figure 12: Comparisons between the observations from the different IMB buoys and the simulations from the multiple linear regression.

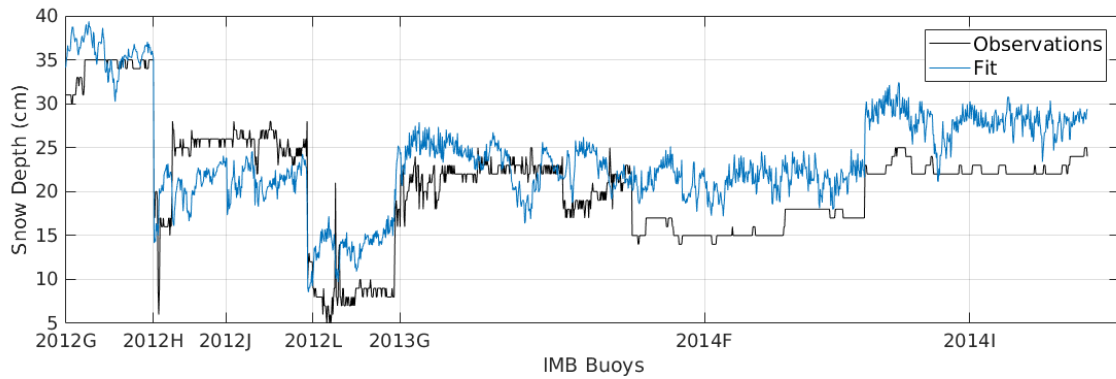
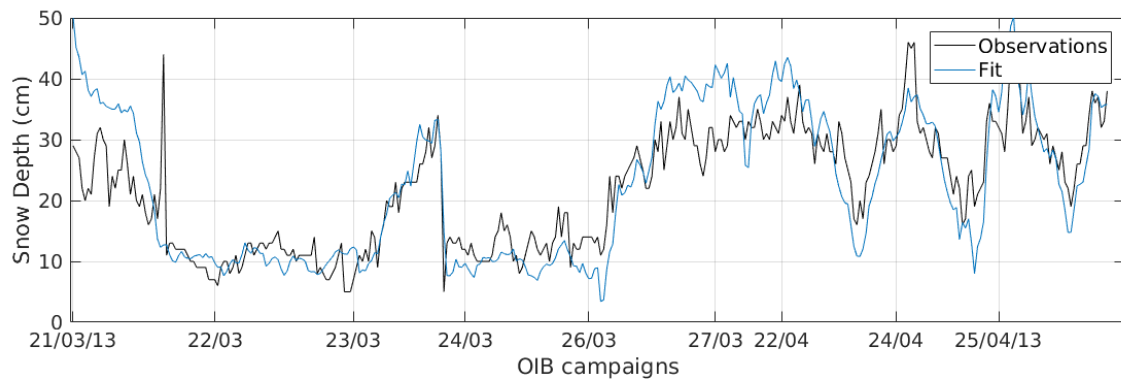


Figure 13: Comparisons between the measurements of snow depth done during 2013 OIB campaigns and the simulations from the multiple linear regression using AMSR2 observations.



from our model and the snow-ice interface temperature given by the simulated data of MEMLS model. It was expected and an equation between TSI from MEMLS simulations and TSI from our empirical model is given :

$$TSI_{sim} = TSI_{empirical\ model} - 5 \quad (11)$$

Where TSI is expressed in K.

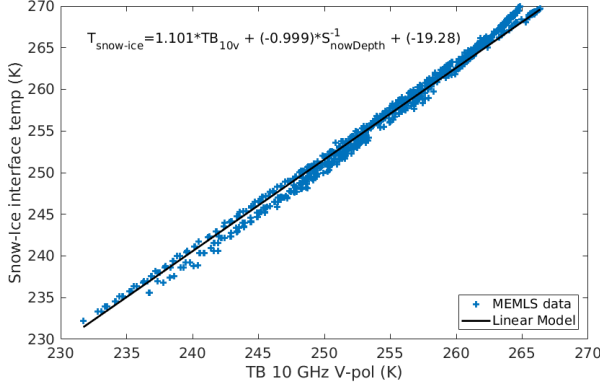


Figure 14: Snow ice interface temperature from memls data as a function of the brightness temperature at 10.65 GHz in blue points, and the multi-linear regression for the mean snow depth in black line.

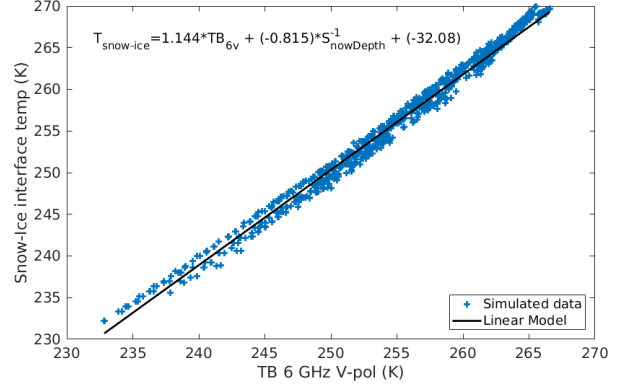


Figure 15: Snow ice interface temperature from memls data as a function of the brightness temperature at 6.9 GHz in blue points, and the multi-linear regression for the mean snow depth in black line.

Then linear regression between the snow-ice interface temperature of simulated and the effective temperature of simulated data at different channels is done. Results are shown on Figure 16. For each channel the coefficients of the linear regression changes. We note that the slope coefficient increases with frequency. So the sensitivity of the Teff to the TSI is increasing, and the sensitivity to noise is also increasing as a function of frequency.

The equations for each channel are given here with the RMSE :

$$\begin{aligned}
 T_{eff\ 6.9V} &= 0.888 \times T_{Snow-Ice_{sim}} + 30.245, & rmse &= 0.891 \\
 T_{eff\ 10.65V} &= 0.901 \times T_{Snow-Ice_{sim}} + 26.569, & rmse &= 0.755 \\
 T_{eff\ 18.7V} &= 0.920 \times T_{Snow-Ice_{sim}} + 21.536, & rmse &= 0.6317 \\
 T_{eff\ 23.8V} &= 0.932 \times T_{Snow-Ice_{sim}} + 18.417, & rmse &= 0.566 \\
 T_{eff\ 36.5V} &= 0.960 \times T_{Snow-Ice_{sim}} + 10.902, & rmse &= 0.410 \\
 T_{eff\ 50V} &= 0.989 \times T_{Snow-Ice_{sim}} + 2.959, & rmse &= 0.320 \\
 T_{eff\ 89V} &= 1.0604 \times T_{Snow-Ice_{sim}} - 16.384, & rmse &= 0.920
 \end{aligned} \quad (12)$$

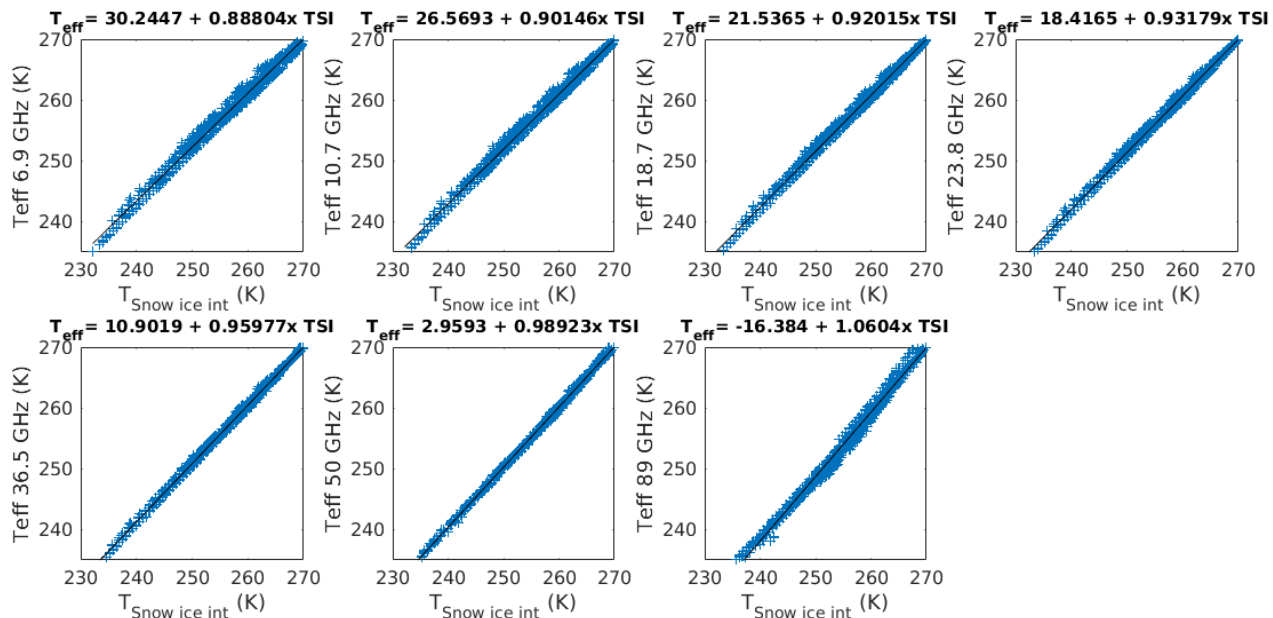
Where TSI and Teff are expressed in K.

Note that the linear regression of Teff at the 50 GHz channel has the lowest RMSE and the one at the 89 GHz channel has the highest RMSE.

## 5 Conclusion

Equations for the snow-ice interface temperature, the effective temperature and the snow depth in terms of brightness temperatures were estimated using RRDP data. The snow-ice interface temperature and the

Figure 16: Relation between the snow ice interface temperature and the effective temperature at different frequencies. The data are in blue points and the linear regression in black line.



snow depth are needed for estimating the effective temperature. Multi-linear regressions have been used. A parametric equation was found for TSI giving an error of 2.11 K when using the 10.65 GHz channel and 2.22 K when using the 6.9 GHz. The multi-linear model to estimate the snow depth from 6.9, 18.7 and 36.5 GHz channels, gives an error of 0.05 m. The linear regression equations to estimate the  $T_{\text{eff}}$  at different microwave frequencies as function of the TSI are presented. This work gives the keys to derive the  $T_{\text{eff}}$  from the microwave TBs. These new  $T_{\text{eff}}$  estimations can be used for correcting brightness temperature over ice in order to compute sea ice concentration.

I recommend that the estimated effective temperature at 50 GHz is implemented into the OSI-404 sea ice emissivity product, and that the effective temperature at 18.7, 36.5 and 89 GHz is used, for correcting the brightness temperatures before computing the sea ice concentration in OSI 401 and OSI 408.

## 6 Acknowledgement

I would like to acknowledge the support from the EUMETSAT OSISAF visiting scientist programme. I would also like to thank the Danish Meteorological Institute (DMI) that welcomed me during this project.

## References

- P. Berrisford, P. Kållberg, S. Kobayashi, D. Dee, S. Uppala, A. J. Simmons, P. Poli, and H. Sato. Atmospheric conservation properties in ERA-Interim. *Q. J. R. Meteorol. Soc.*, 137(659):1381–1399, jul 2011. ISSN 00359009. doi: 10.1002/qj.864.
- J. Comiso, D. Cavalieri, and T. Markus. Sea ice concentration, ice temperature, and snow depth using AMSR-E data. *IEEE Trans. Geosci. Remote Sens.*, 41(2):243–252, feb 2003. ISSN 0196-2892. doi: 10.1109/TGRS.2002.808317.
- I. Grönfeldt. Snow and sea ice temperature profiles from satellite data and ice mass balance buoys. Master’s thesis, Lund University, 2015.
- T. Markus and D. J. Cavalieri. Snow Depth Distribution Over Sea Ice in the Southern Ocean from Satellite Passive Microwave Data in Antarctic Sea Ice: Physical Processes, Interactions and Variability (ed M. O. Jeffries). pages 19–39. American Geophysical Union, Washington, D. C, mar 1998. ISBN 9781118668245. doi: 10.1029/AR074p0019.
- C. Mätzler and A. Wiesmann. Documentation for MEMLS, Version 3, Microwave Emission Model of Layered Snowpacks. Technical report, Tech. rep., Institute for Applied Physics, University of Bern, Switzerland, 2012.
- L. T. Pedersen and R. Saldo. Sea ice concentration (sic) round robin data package. Technical report, European Space Agency, 05 2016.
- D. K. Perovich, J. A. Richter-Menge, B. Elder, K. Claffey, and C. Polashenski. Observing and understanding climate change: monitoring the mass balance, motion, and thickness of Arctic sea ice. Cold Regions Research and Engineering Laboratory, 2017.
- M. Sturm, D. K. Perovich, and J. Holmgren. Thermal conductivity and heat transfer through the snow on the ice of the beaufort sea. *Journal of Geophysical Research: Oceans*, 107(C10), 2002.
- R. T. Tonboe. The simulated sea ice thermal microwave emission at window and sounding frequencies. *Tellus A*, 62(3):333–344, may 2010. ISSN 02806495. doi: 10.1111/j.1600-0870.2010.00434.x.
- R. T. Tonboe, G. Dybkjær, and J. L. Høyer. Simulations of the snow covered sea ice surface temperature and microwave effective temperature. *Tellus A Dyn. Meteorol. Oceanogr.*, 63(5):1028–1037, jan 2011. doi: 10.1111/j.1600-0870.2011.00530.x.

## A Appendix

### A.1 Function to detect the level of the snow-ice and snow-air interfaces

```
function [ levelSAint,levelSIint ] = find_SA_and_SI( tprof )
%This function find the level of the air-snow interface and the snow-ice
%interface
%tprof : matrix containing the temperature profile,
%each column correspond to a level in the profile and each row correspond
%to observations
%levelSAint : vector containing the level of Air-Snow interface for each
%observation
%levelSIint : vector containing the level of Snow-ice interface for each
%observation

slopeprof=zeros(size(tprof,1),size(tprof,2));
for i=1:size(slopeprof,1)
    for j=2:size(slopeprof,2)-1
        %compute temperature gradient
        slopeprof(i,j)=tprof(i,j+1)-tprof(i,j-1);
    end
end
slopeprofdiff=zeros(size(tprof,1),size(tprof,2));
levelSIint=zeros(size(tprof,1),1);
levelSAint=zeros(size(tprof,1),1);

for i=1:size(slopeprof,1)
    for j=3:size(slopeprof,2)-2
        %compute derivative of the temperature gradient
        slopeprofdiff(i,j)=slopeprof(i,j+1)-slopeprof(i,j-1);
    end

    %localize the slopes changements
    [~,pic1]=min(slopeprofdiff(i,:));
    [~,pic2]=max(slopeprofdiff(i,:));
    levelSAint(i)=min([pic1 pic2]);
    levelSIint(i)=max([pic1 pic2]);
end
end
```

### A.2 Function to read IMB CRREL data from RRDP database

```
function [ Cmat ] = read_RRDP_IMBCRREL(filename)
%read_RRDP_IMBCRREL
% this function permit to read the files of the Round Robin Database
%containing IMB CRREL data
%filename : the name of the file containing the data
%Cmat : the ouput matrix containing the data

isstring=[ 4 9 34 35 61 79 84 85 91];%columns of the file which are strings
istime=[3 6 33 60 83];% columns of the file which are time data
```



```

istime=[3 22 49 72];% columns of the file which are time data
%create the format of the data file
fmt = cell( 1, 80 ) ;
fmt(:) = {'%s'} ;
fmt = [fmt{:}] ;

%open the file
fileID = fopen(filename);
%read variables of the file as strings
C= textscan(fileID,fmt,'headerlines', 2,'delimiter',',','');
fclose(fileID);

col=length(C);
row=length(C{1,1});

%Create a numeric matrix which contains the data except strings data (put
%to 0)
Cmat=zeros(row,col);
nanval={'noval',' noval',' noval',' noval',' noval',' noval',' noval'};
for j=1:col
    if sum(j==isstring)==1
        Cmat(:,j)=0;
    else
        for i=1:row
            if sum(j==istime)==1

                Cmat(i,j)=datenum(C{j}(i),'yyyy-mm-ddTHH:MM:SSZ');

            else
                if sum(strcmp(C{j}(i),nanval)==1)
                    Cmat(i,j)=NaN;
                else
                    Cmat(i,j)=str2double(C{j}(i));
                end
            end
        end
    end
end
end
end
end
end

```